AFRL-AFOSR-JP-TR-2018-0066

Synthesis and Characterization of Ionic Chiral Liquid Crystal Monomers and Assessment of their Contribution to Enhanced Performance of Polymer Stabilized Cholesterol Liquid Crystals

Kwang-Un Jeong
CHONBUK NATIONAL UNIVERSITY
567 Baekje-daero, Deokjin-gu
Chonju, Chonbuk, 54896
KR

09/11/2018
Final Report

Air Force Research Laboratory
Air Force Office of Scientific Research
Asian Office of Aerospace Research and Development
Unit 45002, APO AP 96338-5002

REPORT DOCUMENTATION PAGE	*Form Approved* *OMB No. 0704-0188*

1. REPORT DATE *(DD-MM-YYYY)* 11-09-2018	**2. REPORT TYPE** Final	**3. DATES COVERED** *(From - To)* 09 Sep 2017 to 08 Sep 2018

4. TITLE AND SUBTITLE Synthesis and Characterization of Ionic Chiral Liquid Crystal Monomers and Assessment of their Contribution to Enhanced Performance of Polymer Stabilized Cholesterol Liquid Crystals	**5a. CONTRACT NUMBER**
	5b. GRANT NUMBER FA2386-17-1-4078
	5c. PROGRAM ELEMENT NUMBER 61102F
6. AUTHOR(S) Kwang-Un Jeong	**5d. PROJECT NUMBER**
	5e. TASK NUMBER
	5f. WORK UNIT NUMBER
7. PERFORMING ORGANIZATION NAME(S) AND ADDRESS(ES) CHONBUK NATIONAL UNIVERSITY 567 Baekje-daero, Deokjin-gu Chonju, Chonbuk, 54896 KR	**8. PERFORMING ORGANIZATION REPORT NUMBER**
9. SPONSORING/MONITORING AGENCY NAME(S) AND ADDRESS(ES) AOARD UNIT 45002 APO AP 96338-5002	**10. SPONSOR/MONITOR'S ACRONYM(S)** AFRL/AFOSR IOA
	11. SPONSOR/MONITOR'S REPORT NUMBER(S) AFRL-AFOSR-JP-TR-2018-0066

12. DISTRIBUTION/AVAILABILITY STATEMENT
A DISTRIBUTION UNLIMITED: PB Public Release

13. SUPPLEMENTARY NOTES

14. ABSTRACT

The PI had good success with this grant. Ionic and chiral monomers were newly synthesized and applied for the development of polymer-stabilized CLC films which can be tuned by electric fields. The effect of ions in CLC films on the electro-optical properties was especially examined by varying critical parameters ranging from ionic interaction, network density, and helical twisting power. The acrylate function introduced both in ionic and chiral was helpful to securely preserve the self-assembled helical superstructures and to obtain the heterogeneous pitch distributions by the photopolymerization process. Information obtained in this project can be utilized to understand the dynamics of structure development and to better control responses. The large and reversible notch broadening had potential applications for full color displays, broadband polarizers and waveplates.

15. SUBJECT TERMS
cholesteric liquid crystal, chirophotonic crystals, novel ionic monomers

16. SECURITY CLASSIFICATION OF:			**17. LIMITATION OF ABSTRACT**	**18. NUMBER OF PAGES**	**19a. NAME OF RESPONSIBLE PERSON**
a. REPORT	**b. ABSTRACT**	**c. THIS PAGE**			CHEN, JERMONT
Unclassified	Unclassified	Unclassified	SAR		**19b. TELEPHONE NUMBER** *(Include area code)* 315-227-7007

Standard Form 298 (Rev. 8/98)
Prescribed by ANSI Std. Z39.18

Synthesis and Characterization of Ionic Chiral Liquid Crystal Monomers and Assessment of their Contribution for the Enhanced Performances of Polymer-Stabilized Cholesterol Liquid Crystals

- BAA Name: AFRL-AFOSR-2016-0007
- Relevant Section: Organic Materials Chemistry
- Principle Investigator: Kwang-Un Jeong
- Key Researcher involved in the Project: Timothy J. White
- Period-of-Performance: 1 year
- Total Cost: 60,000 US dollars

1. ABSTRACT

Since a cholesteric liquid crystal (CLC) has helical superstructures, the fabrication of photonic crystal material with CLC has been of great interest. When the CLC molecules are aligned parallel to the optical cell, films can show the selective reflection of light depending on the helical pitch. To apply CLC materials in dynamic polarizers, switchable mirrors and data storages, reconfigurable bandwidths and mechanical robustness are required. Therefore, polymer-stabilized CLCs have been widely discussed to develop the flexible optical films and fibers. They possess not only the orientational properties of anisotropic molecules but also the elastic behaviors of polymeric networks. In this work, we newly designed and synthesized novel ionic monomers (IM) and chiral monomers (CM) to demonstrate the polymer-stabilized CLC film showing the enhanced optical performance. By introducing IM and CM into the host achiral LC media, the helical superstructures are automatically constructed by the self-assembly processes. After the ultraviolet (UV) light curing process, a bandwidth broadening can be achieved due to the polymerization-induced phase separation. The research work here is to explore the fundamental relationships between ionic polymer, helical pitch and selective reflection.

2. INTRODUCTION

Color is one of the sophisticated ways to express the intuitive communications and displaying information. Photonic crystals unveiled in nature can offer material scientists to inexhaustible opportunities to generate the colors by developing the novel materials. Among them, a CLC is an attractive material because its spontaneous self-assembly constructs the periodic nanostructure. The CLC reflects vivid and bright color in the selective region. To control the magnitude and bandwidth of wavelength of reflective light, the photopolymerization of CLC has been reported. In the case of the homogeneous photopolymerization, polymer network was formed to freeze the initial helical pitches. However, the heterogeneous photopolymerization dictates the gradients in the cross-link density of the polymer network. This CLC polymeric system reaches the variation in the position and bandwidth. This project demonstrates the fabrication of robust reflector which can be stabilized via the in situ photopolymerization of chiral and ionic reactive mesogen (RM) in host nematic media. This work is to elucidate the powerful role of ions in the polymer network and to illustrate the potential functionality of bandwidth broadening of CLC film. A series of chiral and ionic RM is synthesized and a variety of formulations are examined to enable optimal optic property. The control of CLC reflection is potentially useful in many application areas, such as displays, paints, smart windows, and photo-communication materials.

3. EXPERMENTAL SECTION

3.1. Materials

4,4'-Biphenol (99%, Sigma), 1,8-dibromooctane (99%, Sigma), triethylamine (TEA, 99%, Sigma), N-(3-(dimethylamino)propyl)-N'-ethylcarbodiimide hydrochloride (99%, TCI), 4-(dimethylamino)pyridine (99%, TCI), (*R*)-1-(2-naphythyl)-ethanol (98%, Sigma), 1-(2-hydroxynaphthalen-1-yl)naphthalen-2-ol (98%, Sigma), anhydrous tetrahydrofuran (THF, 99.9%, Sigma), anhydrous methylene chloride (MC, 99.9%, Sigma), absolute ethanol (EtOH, 99.5%, Sigma-Aldrich), ethyl acetate (EA, 99.9%, Samcheon Chem.), chloroform ($CHCl_3$, 99.9%, Samcheon Chem.), hydrochloric acid (HCl, 37%, Sigma), sodium hydroxide (NaOH, 93%, Showa), potassium carbonate (K_2CO_3, 99%, Showa), anhydrous magnesium sulphate ($MgSO_4$, 99.5%, Showa), and nematic liquid crystal (E7, Merck Co.) were used as received

3.2. Characterization

Chemical structure and purity of ionic and chiral reactive mesogen were confirmed by proton (^{1}H) nuclear magnetic resonance (NMR, JEOL JNM-EX400). Chemical shifts were quoted in part per million (ppm) with a reference of tetramethylsilane (TMS). Molecular weight was confirmed by matrix-assisted laser desorption and ionization time-of-flight mass spectroscopy (MALDI-ToF MS, Voyager DE PRO). Matrix of 2,5-dihyroxybenzoic acid (DHB, Aldrich) was used on a spectrometer. Elemental analysis was performed by an EA1110 (CE instrument). The analysis of results was determined by the ratio of elements within the sample, and working out a chemical formula that fits with those results. Thermal transition behavior was studied using differential scanning calorimetry (DSC, Perkin Elmer PYRIS Diamond). For the DSC experiments, the sample weights were controlled to be about 6.0 mg and the pan weights were kept constant with a precision of ± 0.001 mg. The temperature and heat flow scales were calibrated using standard materials at different cooling and heating rates. Heating experiments always preceded the cooling experiments to eliminate previous thermal histories, and the cooling and heating rates were always kept identical. Optical textures of the ordered phases at different temperatures were observed with polarized optical microscopy (POM, Nikon ECLIPSE LV100POL) coupled with a heating stage (Mettler Toledo FP90). The one-dimensional (1D) wide angle X-ray diffraction (WAXD) experiments were conducted in the reflection mode of a Rigaku 12 kW rotating anode X-ray (CuKα radiation) generator coupled with a diffractometer. The diffraction peak positions and widths were calibrated with silicon crystals in the high 2θ-angle region (>15°) and silver behenate in the low 2θ-angle region. To monitor the structural evolutions with temperature changes, a hot stage calibrated to be within ±1 °C error was coupled to the diffractometer. Samples were scanned across a 2θ-angle range of 1.5° to 35° at a scanning rate of 2 °C/min.

3.3 Synthesis of CMR

The compound of 4'-[6-(2-methacryloyloxy)hexyloxy]biphenyl-4-carboxylic acid (0.25 mmol) was added to a solution of N-(3-(dimethylamino)propyl)-N'-ethylcarbodiimide hydrochloride (1.25 mmol) and 4-(dimethylamino)pyridine (1.25 mmol) in 50 mL of tetrahydrofuran/methylene chloride mixed solvent (v/v = 1/4). After being stirred at room temperature for 15 min, (*R*)-1-(2-naphythyl)-

ethanol (1.0 mmol) was introduced as a solid, and the solution was stirred at room temperature for 48 h. After distillation, the residue was dissolved in chloroform and washed with water several times. The crude product was purified by column chromatography on silica gel using ethyl acetate/methylene chloride = 1:4 to yield CMR (Yield: 72%).

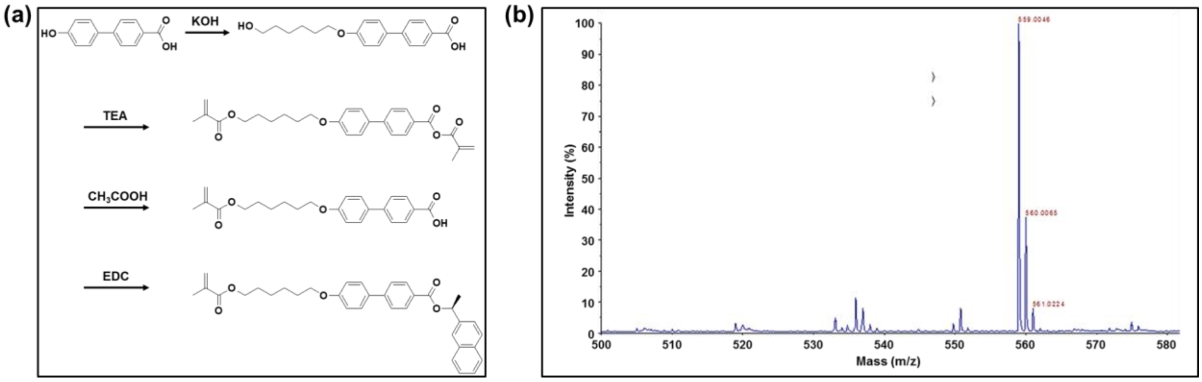

Figure 1. Synthetic procedure (a) and MALDI-ToF mass spectra (b) of CMR.

3.4. Synthesis of CDR

The compound of 4-(5-(acryloyloxy)pentyloxy)benzoic acid (0.55 mmol) was added to a solution of N-(3-(dimethylamino)propyl)-N'-ethylcarbodiimide hydrochloride (2.20 mmol) and 4-(dimethylamino)pyridine (2.20 mmol) in 100 mL of chloroform. After being stirred at room temperature for 15 min, 1-(2-hydroxynaphthalen-1-yl)naphthalen-2-ol (0.15 mmol) was introduced as a solid, and the solution was stirred at room temperature for 48 h. The organic phase was washed with distilled water and then extracted. The crude product was purified by column chromatography on silica gel using ethyl acetate/methylene chloride = 1:12 to yield CDR (Yield: 81%).

3.5. Synthesis of 4,4'-bis((8-bromooctyl)oxy)-1,1'-biphenyl

4,4'-Biphenol (21.5 mmol), 1,8-dibromooctane (86 mmol), and potassium hydroxide (43.0 mmol) were dissolved in 300 mL ethanol and refluxed for 12 h at 70 °C under N_2 atmosphere. After cooling to the room temperature, the crude product immediately precipitated and was filtered. The precipitates washed with ethanol and water several times. White solids were obtained by recrystallization in tetrahydrofuran. (Yield: 73 %)

3.6. Synthesis of MBIR

4,4'-bis((8-bromooctyl)oxy)-1,1'-biphenyl (1.77 mmol) was dissolved in cosolvents consisting of 40 mL of acetonitrile and 20 mL of chloroform. 2-(Dimethylamino)ethyl methacrylate (7.08 mmol) was added to the solution and refluxed for 3 days at 60 °C. Excess of diethyl ether was poured into the flask, following elimination of organic solvents. The suspension was sonicated in an ultrasound bath for 30 min. The precipitate was filtered and washed with diethyl ether. White solids were obtained after dried under vacuum. (Yield: 90 %)

3.7. Synthesis of 4-((8-bromooctyl)oxy)-1,1'-biphenyl

4-phenylphenol (23.52 mmol), 1,8-dibromooctane (47.04 mmol), and potassium hydroxide (23.52 mmol) were dissolved in 250 mL of ethanol and refluxed for 12 h at 70 °C under N_2 atmosphere.

After reaction, the crude product immediately formed upon cooling and was filtered. The precipitate washed with ethanol and water several times, subsequently was dried under vacuum to afford the product as a white solid. (Yield: 73 %)

3.8. Synthesis of DBIR

4-((8-Bromooctyl)oxy)-1,1'-biphenyl (2.78 mmol) was dissolved in cosolvents consisting of 30 mL of acetonitrile and 15 mL of chloroform. 2-(Dimethylamino)ethyl methacrylate (3.61 mmol) was added to the solution and refluxed for 3 days at 60 °C. After evaporation of the solvent, excess of diethyl ether was poured into the flask. The suspension was sonicated in an ultrasound bath for 30 min. The precipitate was filtered and washed with diethyl ether. White solids were obtained after dried under vacuum. (Yield: 95 %)

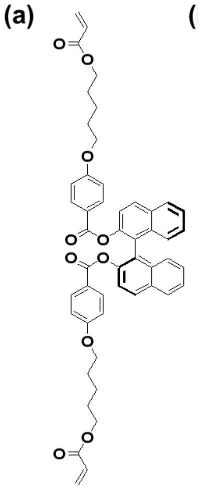

(b)

	experimental content (%)	calculated content (%)
C	74.15 74.09 74.01	74.43
H	5.64 5.52 5.48	5.75
O	- - -	19.83

Figure 2. Chemical structure (a) and elemental analysis (b) of CDR.

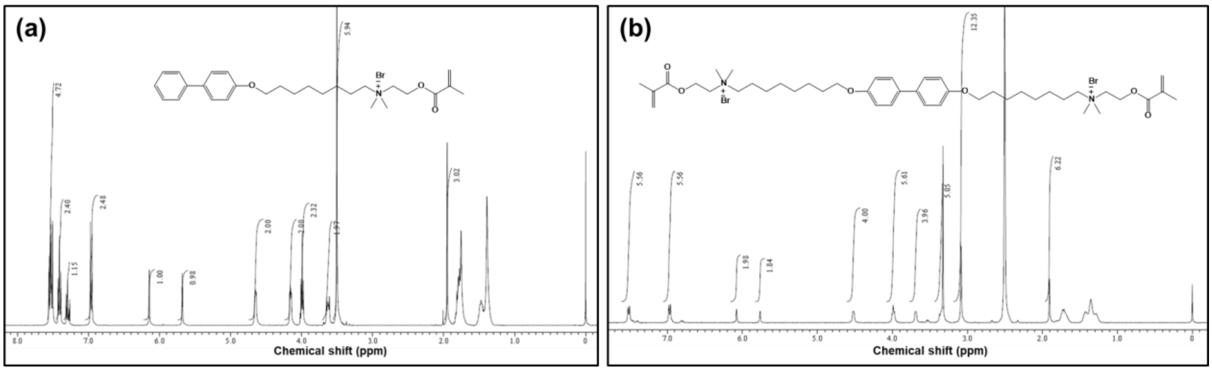

Figure 3. ^{1}H NMR spectra of MBIR (a) and DBIR (b).

4. RESULTS AND DISCUSSION

4.1. Programmed Reactive Mesogen

The chiral reactive mesogen (RM) abbreviated as CMR containing both chemically photopolymerizable methacrylate group and chiral (*R*)-configured naphthyl unit was designed and synthesized (Figure 1a). The hydrocarbon chain and biphenyl mesogen covalently connecting to the both side of reactive group and chiral unit enhances the compatibility not only in the isotropic organic solvent but also in the anisotropic nematic host. Chemical structure of CMR was identified by MALDI-ToF mass spectrometry (Figure 1b). Since the CRM molecules were programmed to take into account the intramolecular conformations and intermolecular interactions, a new class of chiral RM enable the formation of cholesteric liquid crystal (CLC) phase in the nematic medium that induce a rotation of nematic director. The CDR molecule was obtained by the esterification reaction of alcohol with acid in the presence of EDC and DMAP with high yield and purity. The aromatic core was specifically selected as a chiral group to induce strong helical twisting power due to its axial chirality. The molecular weight of the CDR was 806.89 g/mol (Figure 2). Generally, the biphenyl-based derivatives had a high compatibility with LC molecules. To enhance the phase separation behavior to that of anisotropic media, we chemically introduced the charged groups at the ends of RM. When the ionic interactions were balanced with the π-π interaction and Van der Waals force, these RM molecules were initially dissolved and spontaneously self-assembled. Chemical structures and purities of the MBIR and DBIR were confirmed by ^{1}H NMR (Figure 3).

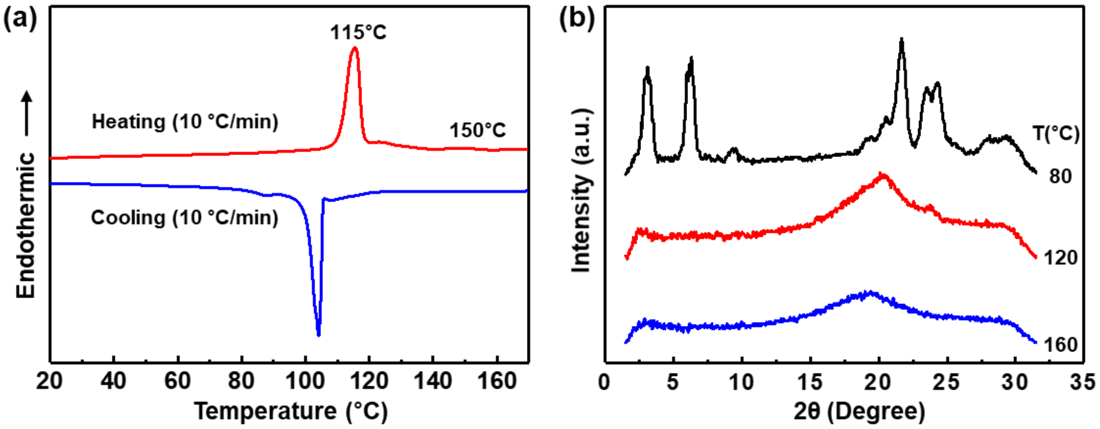

Figure 4. DSC thermogram (a) and XRD patterns (b) of DBIR.

4.2. Phase Transformation and Ordered Structure

The DSC experiment was conducted at cooling and heating rates of 10 °C/min to determine the thermal transition temperatures and quantitative thermodynamic property. As shown in Figure 4, DBIR showed multiple phase transitions in the bulk. After crystal melting over 115 °C, the LC mesophase appeared, which in turn undergoes isotropization at 150 °C. Moreover, two endothermic peaks detected during heating were consistent with those of the cooling process. It indicated that DBIR exhibited enantiotropic phase transitions (Figure 4a). To obtain structural information, powder patterns of 1D WAXD were obtained. As shown in Figure 4b, DBIR was in the isotropic state at 160 °C, exhibiting only amorphous halos. At 120 °C, apparent amorphous halo was observed at the high angle region. A diffraction halo corresponded to the quasi long-range correlation of the biphenyl groups. The broad signal was mainly attributed to the partially molten alkyl chains in the side portion. At 80 °C, many reflection peaks were developed owing to the formation of a highly ordered crystal phase. Particularly, in the high angle region, the scattering in the LC phase was split into sharp distinct diffraction peaks that lateral organization between the molecules increased dramatically.

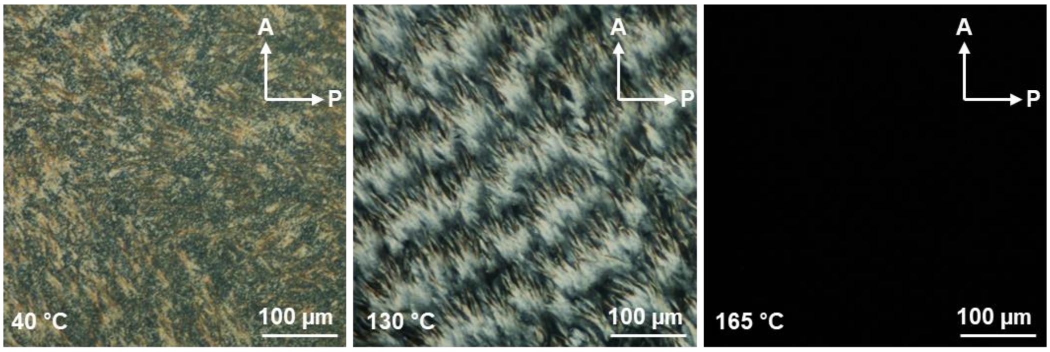

Figure 5. POM images of MBIR at different temperatures.

For the MBIR compound, onset transition at high transition temperature did not show the supercooling effect. This implies that thermodynamic properties of the first-order transition were close to those of the equilibrium state. Upon cooling the MBIR below the lowest thermal transition, the degree of order significantly increased, concomitantly decreasing the symmetry, owing to strong molecular organization. Phase transitions of MBIR were monitored by POM observations at different temperatures (Figure 5). Strong birefringence in the microscopy images of the two ordered phases should be due to the self-assembly of nanophase separated building blocks.

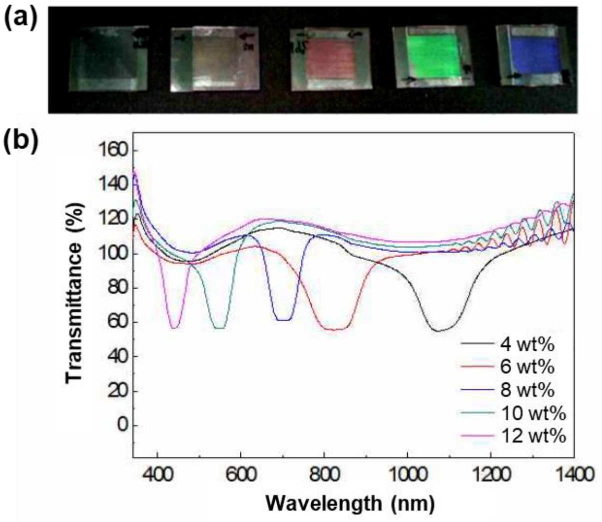

Figure 6. Macroscopic images of CLC films (a) and their light reflection spectra (b).

4.3. Formation of Helical Superstructure

The mixtures of nematic medium with a chiral dopant selectively reflected different colors according to the Bragg's law, $\lambda_{max} = n \times P$, where λ_{max} was the center wavelength for the maximally reflected light, n was the refractive index of host LC, and P was the helical pitch in micrometres. The P was controlled by tuning the concentration of the chiral dopant with different handedness. In this research, two chiral molecules of CMR and CDR with (*R*)-configuration were used to induce CLC phase. By simply dissolving the chiral molecules in the nematic host, the CLC mixtures were prepared and loaded into standard optical cells. For example, CMR (4 wt%), CDR (1 wt%), MBIR (5 wt%), MDIR (1 wt%), and E7 (89 wt%) were mixed with dichloromethante. After solvent was evaporated, the homogeneous mixture was injected into the anti-parallelly rubbed optical cell by capillary action at about 180 °C. After slow cooling to the room temperature, the CLC film was obtained with planar anchoring condition and 10 μm thickness. Note that the concentration of CDR, MBIR, and MDIR was always identical. It indicated the CLC mixture with 6 wt% of CMR was dissolved in 87 wt% of E7. The diacrylate monomer act as the chemical cross-linker. The monoacrylate monomer was purposely added to suppress the crystallization of mesophases by forming the eutectic mixture. The 4 wt%, and 6 wt% of CRM doped CLC mixture reflected the light in the infrared region. There was no detectable color (Figure 6a). To realize its potential in the practical applications for optical devices, the reflection band of CLC film was required to be in visible wavelength. When the 8 wt%, 10 wt%, and 12 wt% of CMR is dissolved into E7, the CLC films exhibited the red, green, and blue, respectively, which was often expected in photonic crystal (Figure 6b). As shown in Figure 7, the CLC film fabricated with flexible optical cell was also tested. The transparent plastic substrate was first coated with polyimide polymer solution and then rubbed to form the planar alignment layer. After thermal curing, the two substrates were sandwiched with 10 μm cell gap spacer and tape. The 12 wt% of CMR mixture revealed blue color. When the CLC film was bent, it still showed the good reflection color. It indicated that the CLC mixture possessed not only with optical property but also with intrinsic viscosity had great potential to apply in the architectural coating and flexible device.

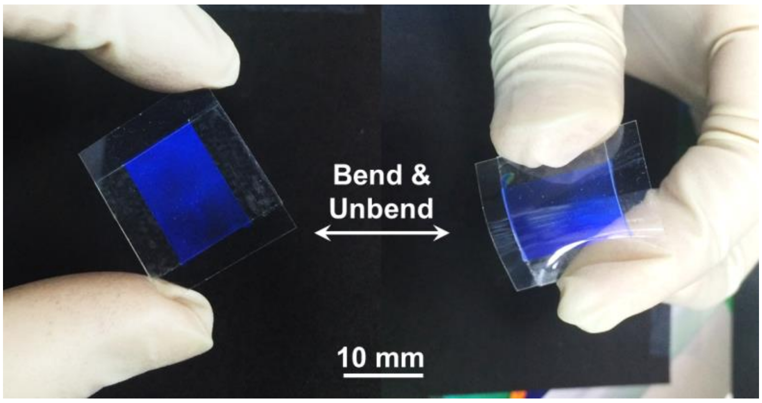

Figure 7. Photographs of CLC film within plastic optical cell in the bend and unbend state.

4.4. Polymerization Induced Helical Pitch Gradient

For this study, the CLC mixture composition of 8 wt% of CRM was used that showed the red color. We assumed that the polymerization induced phase separation led the helical pitch gradient from the upper to lower substrate. First, the CLC mixture were filled into the optical cell, and then they were irradiated by UV light (365 nm) at room temperature for 60 min. Figure 8a showed the transmittance spectra of the samples before and after photopolymerization. Compared with sample that monomeric and polymeric state, it can be observed that the reflection wavelength of the samples was greatly affected. The reflection wavelength of the sample after polymerization was broadened, which was about 400 nm covering from 400 nm to 800 nm, while that of initial sample only reflected at around 600 nm. The influence of the UV light intensity for the CLC films on the reflection wavelength was further confirmed. The slow polymerization rate showed relatively good helical pitch broadening. The mechanism of broadband reflection can be explained by the construction of the gradient distribution of the helix. The gradient in UV intensity over the thickness of the cell was inevitable consequence by forming the polymer network. The upper cell which was near to the UV light source had polymer network first, which resulted in the difference in the polymerization rate at different locations. While the lower side with a lower UV light intensity consumed less content of monomers. As the result of different chiral monomer consumptions, the helical pitch gradient was realized accompanied with the cross-linked network. During the same time, ionic monomer accelerated the phase separation of polymer main chains from the low molecular LC materials. Therefore, the upper and lower side constructed the helical pitch with small and long, respectively. The strong birefringence and oily streak texture detected by POM further supported that the chiral property of the CLC monomers are successfully transferred to the CLC polymers with the helical information (Figure 8b).

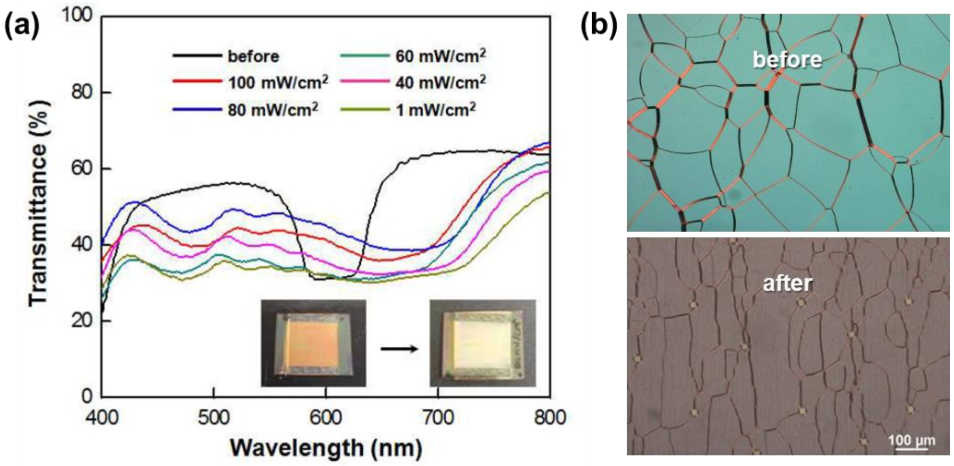

Figure 8. Reflection spectra (a) and POM microphotographs (b) of CLC films before and after photopolymerization.

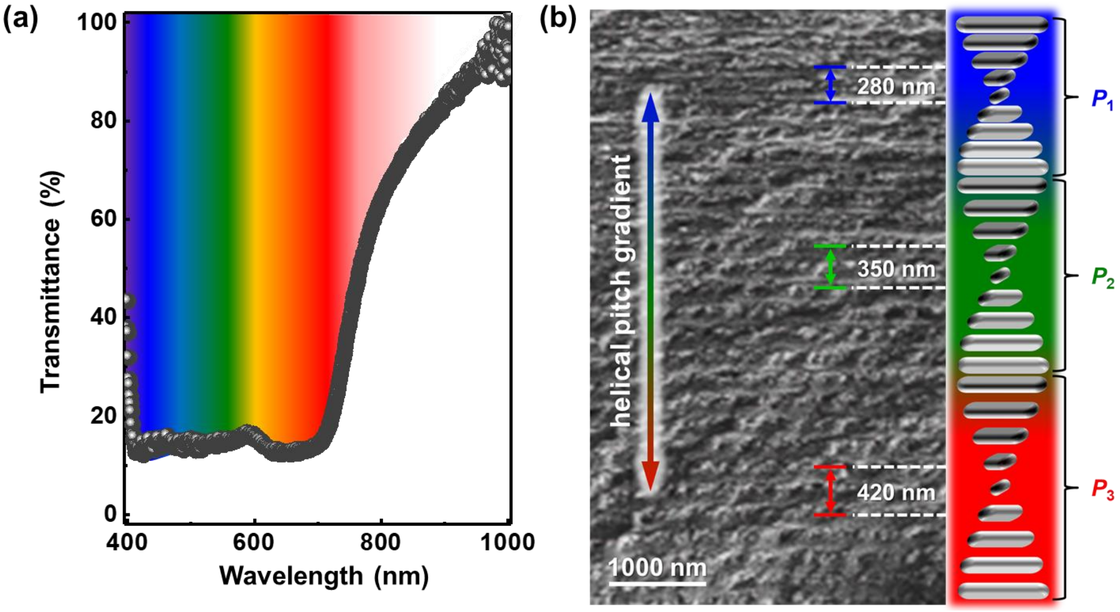

Figure 9. The transmission of the object to right handed circular polarized light (a) and SEM image of the fractured surface (b) of CLC films.

4.5. Morphological Observation of Helical Superstructures

Derived from the nascent properties of the chlolesteric mesophase, photopolymerized CLC reflector retained the broadband reflection when probed with right handed (RH) circularly polarized light (CPL). Figure 9a illustrated the change in optical properties as the photonic element was built, ultimately achieving a broad bandwidth ($\Delta\lambda$ = 400 nm) reflection spectrum of RH CPL, which is almost three times the unpolymerized CLC film and covered the entire visible wavelength range. To left-handed (LH) CPL the light was transmitted and no reflection color was observed. To visualize the distinct helical superstructures within the broadband mirrors, a SEM was employed. As shown in Figure 9b, the cross-sectional SEM image of the CLC film has a 10 µm thick layer. The representative lengths of P_1 = 280 nm, P_2 = 350 nm, and P_3 = 420 nm were measured according to the blue, green, and red light reflecting layers, respectively. It can be found that the CLC film exhibited the pitch gradient distribution over the thickness of the cell. That was a shorter pitch at the upper side while a longer one at the lower side, as shown in the picture: $P_3 > P_2 > P_1$. The above experimental results provided an important support for our explanation.

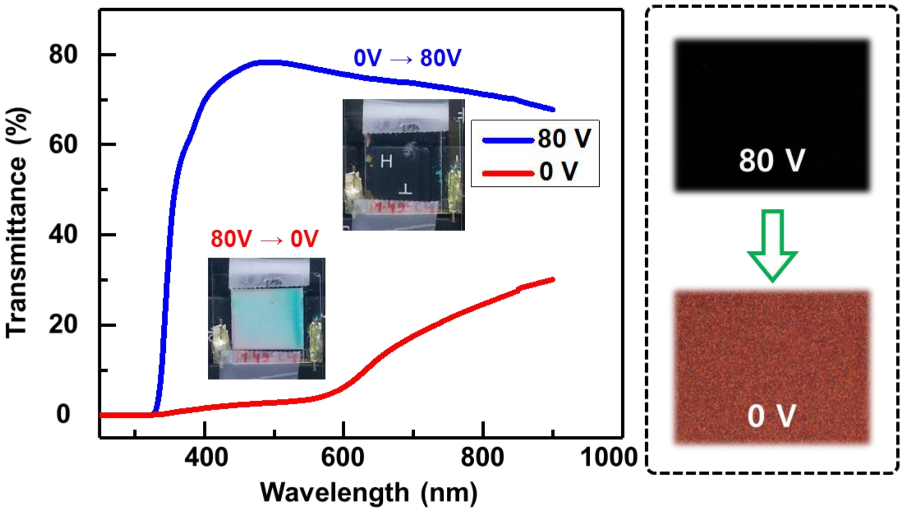

Figure 10. Transmittance change of CLC film by applying the electric field.

4.6. Electro Optical Responsive of CLC Films

To test the electro optical properties of CLC film, the photopolymerized cell was prepared. Without electric fields, the well dispersed and homogeneously oriented nematic media formed along the helical superstructure were effective in reflecting visible light, which results in a white state (Figure 10). By applying an electric field above 80 V, a dark state was obtained in the macroscopic region. This observation indicated that the long axis of anisotropic molecules was oriented parallel to the vertically applied electric field above 80 V and generated a homeotropically aligned state. It should be noted that 80 V was the applied voltage for a maximum transmittance state measured by voltage transmittance curves. The perfect dark phase with the CLC film was shown in homeotropic alignment. The light reflecting state of CLC film was switched to a transmittance state by applying the electric field.

6. CONCLUSION

Ionic and chiral monomers were newly synthesized and applied for the development of polymer-stabilized CLC films which can be tuned by electric fields. The effect of ions in CLC films on the electro-optical properties was especially examined by varying critical parameters ranging from ionic interaction, network density, and helical twisting power. The acrylate function introduced both in ionic and chiral was helpful to securely preserve the self-assembled helical superstructures and to obtain the heterogeneous pitch distributions by the photopolymerization process. Information obtained in this project can be utilized to understand the dynamics of structure development and to better control responses. The large and reversible notch broadening had potential applications for full color displays, broadband polarizers and waveplates.